*Egypt. J. Chem.* **Vol. 64**, No. 4 pp. 1911 - 1926 (2021)

**Egyptian Journal of Chemistry**

**http://ejchem.journals.ekb.eg/**

# Effect of Elevated Temperatures on The Performance of Metakaolin Geopolymer Pastes Incorporated by Cement Kiln Dust

**Nourhan N. Kassem[1], Doaa A. Ahmed[2] and Essam A. Kishar[2]**

*Faculty of Women for Arts, Science and Education Ain Shams University,*

*Asmaa Fahmi St Al Golf, Nasr City, Cairo, 11566, Egypt*

**Abstract**

The aim of the present work was to study the influence of elevated temperatures on the thermal behavior of geopolymer cements based on the incorporation of metakaolin with cement kiln dust. Geopolymer composites were synthesized by partially substituted metakaolin (MK) with 0, 20, 30 and 40 wt% of cement kiln dust (CKD). The mixture of liquid sodium silicate ($Na_2SiO_3$) and sodium hydroxide (NaOH) was used as alkaline activator solution with fixed ratio 2.5 and the concentration of sodium hydroxide was 10 Molar. The obtained geopolymer specimens were cured in water at ambient temperature (25°C) for 28 days and then subjected to various elevated temperatures 200, 400, 600 and 800°C for one hour. Geopolymer cements were characterized before and after temperature exposure via visual appearance, X-ray diffraction (XRD), Fourier Transform infrared spectrometry (FTIR) and the compressive strength test. Some selected samples were investigated by using thermo gravimetric analysis (TGA/DTG).The results show that, all geopolymer specimens loss their compressive strength from ambient temperature to 400°C. This is due to the escape of moisture and dehydroxylation of aluminosilicate gel from the geopolymer matrix. However, geopolymer samples gained strength upon heating to 600°C as a result of further polymerization of unreacted silicate species. At 800°C, the geopolymer mix with 20% CKD retained highest strength and thermal stability than other mixes due to viscous sintering process which induced crack healing thus enhanced the mechanical properties of geopolymer under high temperature. This suggests that geopolymer paste that contains 80% MK and 20% CKD can withstand high temperature as well as very suitable for refractory and fire resistance applications.

*Keywords:* Geopolymer Cement ; Metakaolin ; Cement kiln dust ; Elevated Temperature

## 1. Introduction

One of the negative aspects of ordinary Portland cement (OPC) is that it releases large amounts of carbon dioxide ($CO_2$) into the atmosphere by decomposition of limestone during cement manufacture process. The production of one ton OPC lead to formation of about one ton $CO_2$ [1, 2] and this gas is the major contributor to the green house effect and global warming. In that respect, the pursuit to find an alternative cementitious material that can reduce the drawback of Portland cement and has low environmental impacts had become an urgent issue for many recent researches. Geopolymers are regarded as a green alternative construction materials due to their merits over Portland cement such as low energy consumption, low shrinkage [3], excellent mechanical strength [4], less $CO_2$ emission [5, 6] and have superior resistance to fire [3, 7]. Geopolymer can be synthesized from alkaline activation of aluminosilicate source materials that are rich in both silica ($SiO_2$) and alumina ($Al_2O_3$). Among these materials metakaolin is widely used as a pure aluminosilicate source which produced from the calcination of kaolinite clay as a result of losing

*Corresponding author e-mail: nouranabil.eg@gmail.com.; (ORCID ID https://orcid.org/0000-0002-8164-7599).
Received Date 26 November 2020; Revised Date 21 December 2020; Accepted Date 17 January 2021
DOI: 10.21608/EJCHEM.2021.50848.3041

water lattice at a specific temperature ranging from 500°C to 800°C as shown in equation (1) [8].

$Al_2O_3.2SiO_2.2H_2O \rightarrow Al_2O_3.2SiO_2 + 2H_2O$ (1)

Many researches were conducted on the incorporation of metakaolin with industrial waste products such as fly ash (FA) [9, 10], silica fume (SF) [11, 12], ground granulated blast furnace slag (GGBFS) [4, 6] and cement kiln by-pass dust (CKD) [13, 14]. Cement kiln dust is produced in great amounts as a by-product of the cement industry. It contains a high concentration of sulfate and alkalis ($Na_2O$, $K_2O$) which prevents recycling it in cement manufacturing. Frías & Cabrera [15] found that alkaline activation of metakaolin in the presence of free lime produced mainly calcium silicate hydrate (C-S-H), stratlingite ($C_2ASH_8$) and Tetra- calcium aluminate hydrate ($C_4AH_{13}$). At ambient temperature, these phases are stable. However, at elevated temperatures some of them are metastable phases ($C_2ASH_8$ and $C_4AH_{13}$) converting to hydrogarnet ($C_3ASH_6$) [16]. In recent years, several researches studied the thermal behavior of MK-based geopolymer cements under elevated temperatures, but some studies in this field contradictor the other. Rashad et al.[17] investigated the thermal behavior of geopolymer prepared from metakaolin (MK) with partially replaced by quartz powder (QP) at level ranging from 0% to 30% after exposure to different temperatures in the range 400 -1000°C, and they reported that the initial compressive strength for all different pastes increased rapidly at 400°C and then gradually decreased in 600-1000°C due to thermal deformation.

In a contrary study, Tchakouté et al.[18] studied the thermal behavior of geopolymer based on metakaolin using sodium water glass (NWG) from rice husk ash and waste glass as an alkaline activator. They reported rapidly reduction in compressive strength of geopolymer from ambient temperatures until 400°C. While at 600°C the compressive strength increased relatively to 200°C and 400°C, then the compressive strength dropped rapidly at 800°C due to the complete evaporation of chemically bound water. Elimbi et al. [19] found that alkali- activated metakaolin (AAMK) pastes exhibited a loss in the initial compressive strength after subjected to temperature ranging from 300-900°C. Barbosa & MacKenzie [20] examined the effect of elevated temperature on the performance of geopolymer contained metakaolin and sodium silicate and they reported the high thermal stability of metakaolin up to 1200°C. According to Rickard et al. [21] , the geopolymer could be exhibited strength gain after thermal exposure due to the sintering of un-reacted silicate particles.

The objective of the present work is to study the influence of the elevated temperature on the performance of metakaolin based geoplymer paste, in order to develop an optimum MK-CKD binder that can withstand very high temperature. Therefore, this study focuses on the thermal stability of geopolymer pastes prepared by partially replaced MK with 0, 20, 30 and 40% CKD after exposure to different elevated temperatures 200, 400, 600 and 800°C. Geoplymer cements were characterized via visual appearance, X-ray diffraction (XRD), Fourier Transform infrared spectrometry (FTIR) and the mechanical properties before and after temperatures exposure. Some selected samples were investigated by using thermogravimetric analysis (TGA and DTG).

## 2. Experimental

### *2.1. Materials*

Metakaolin (MK) was supplied by Hemts Construction Chemical Company, Cairo, Egypt. Cement kiln by-pass dust (CKD) was provided by El-Nahda Cement Factory, Qena, Egypt. Those materials are the source of silica and alumina that used for preparing geopolymer specimens. The chemical composition of the raw materials obtained from X-ray fluorescence (XRF) analysis was presented in Table 1. The XRF results exhibited that the major constituents of MK are silica ($SiO_2$) and alumina ($Al_2O_3$) that represent about 95%. Mineralogical characterization of MK was done using X-ray diffraction analysis as shown in Fig. 1.The XRD reveals that MK is composed mainly of illite,

quartz ($SiO_2$), microcline ($KAlSi_3O_8$) and trace amount of anatase ($TiO_2$) as impurities. Elimbi et al. [22] studied the clay minerals and they reported that the main constituent of MK is kaolinite, quartz, illite and anatase as impurities. A mixture of sodium hydroxide (NaOH) and commercial liquid sodium silicate (LSS) was used as the alkaline activator solution. The NaOH flakes with purity 99% were purchased from EL-Goumhouria chemical company, Cairo, Egypt.

**Table1.** Chemical compositions of starting materials.

| Oxide (wt %) | $SiO_2$ | $Al_2O_3$ | $Fe_2O_3$ | CaO | MgO | $SO_3$ | $Na_2O$ | $K_2O$ | $Cl^-$ | $TiO_2$ | $P_2O_5$ | L.O.I | Total |
|---|---|---|---|---|---|---|---|---|---|---|---|---|---|
| MK | 64.80 | 30.10 | 0.55 | 0.52 | ---- | 0.13 | 0.10 | ----- | ----- | 2.70 | 0.06 | 0.73 | 99.69 |
| CKD | 14.16 | 3.98 | 3.42 | 53.87 | 0.86 | 3.68 | 3.01 | 6.62 | 7.43 | ----- | ----- | 2.80 | 99.83 |

solution until a homogeneous paste was reached.

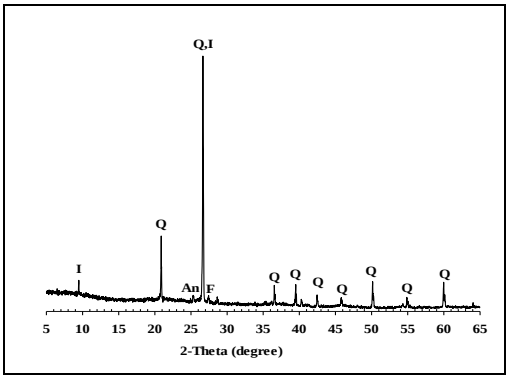


Fig. 1.X-ray pattern for the raw metakaolin
An:anatase ($TiO_2$); F:feldspar ($KAlSi_3O_8$) ;Q:quartz ($SiO_2$); I:illite ($KAl_2SiO_3AlO_{10}$ $(OH)_2$

### *2.2. Geopolymer synthesis*

A combination of liquid sodium silicate $Na_2SiO_3$ and sodium hydroxide NaOH was utilized as an alkaline activator for producing geopolymer cements. The concentration of 10M NaOH was prepared by dissolving NaOH pellets into distilled water and allowed to cool down to room temperature. The alkaline activator solution was prepared 24 hours prior casting. The liquid sodium silicate and sodium hydroxide solution were mixed together with fixed ratio of 2.5:1 until a clear gel was obtained. Based on previous work [6] the concentration of 10 molar NaOH exhibited the best mechanical properties of geopolymer cement. The geopolymer samples were fabricated by replacement metakaolin with different ratios (0, 20, 30 and 40%) of CKD as represented in Table 2. Geopolymer pastes were prepared by mixing raw materials of each mix with the alkaline activator

After mixing, the fresh pastes were rapidly cast into a cubic mould with a dimension of 25x25x25 $mm^3$. The mould was vibrated to remove the entire air bubbles and then left undisturbed in humidity (100% R.H.) under room temperature for 24 hours. After this period, the cubes were demolded and cured under tap water in a tight plastic container at ambient temperature for 28 days. At the end of the curing regime, the specimens were removed from their curing conditions and subjected to the compressive strength measurements [23]. The hydration reaction was stopped by taking the resulting crushed specimens and stirred with stopping solution of alcohol / acetone (1:1) for preventing further hydration [24, 25] followed by drying of the crushed specimens for 24 hours at 80°C, then kept for analysis.

**Table 2.** Mix composition, water/solid (L/S) ratio and setting times

| Mix | MK (%) | CKD (%) | MK (grams) | CKD (grams) | $Na_2SiO_3$ solution (grams) | NaOH Solution (grams) | $Na_2SiO_3$ : NaOH | L/S ratio | Initial setting time (Min) | Final setting time (Min) |
|---|---|---|---|---|---|---|---|---|---|---|
| $M_0$ | 100 | --- | 1500 | ----- | 605 | 242 | 2.5 | 0.56 | >1 day | // |
| $MD_{20}$ | 80 | 20 | 1200 | 300 | 640 | 256 | 2.5 | 0.59 | 35 | 44 |
| $MD_{30}$ | 70 | 30 | 1050 | 450 | 678 | 270 | 2.5 | 0.63 | 23 | 30 |
| $MD_{40}$ | 60 | 40 | 900 | 600 | 718 | 287 | 2.5 | 0.67 | 18 | 26 |

On the other hand, after 28 days the specimens were subjected to different elevated temperature 200, 400, 600 and 800°C in an electrical furnace with a heating rate 10°C/min, a hold time of one hour, and then were cooled at ambient temperature to determine the residual compressive strength. The oxide content of the starting raw materials was verified by using XRF spectrometer (ARL9900). The phase characteristics were investigated by using X-ray diffraction analysis. The XRD was carried out with empyrean diffractometer using Ni- filtered and Cu-Kα radiation of wavelength λ= 1.5418Ao and pixel detector operating at the following condition; voltage 40 kv and current 40 mA. The XRD scales of 2Θ value in the range from 4o to 65o with step size 0.013 at scanning rate of 2o per minute, at National Institute of Standards NIS ,Giza, Egypt. The Fourier Transform Infrared Spectroscopy (FTIR) measurements are carried out on Perkin - Elmer - 1430 infrared spectrophotometer using potassium bromide (KBr) pellets, about 2mg of the sample was grinded with 20-fold of KBr (dried in an oven prior to its use) and then pressed in the form of a disc, in order to evaluate the shifting of functional groups, at Micro-Analytical central, Ain Shams University, Egypt. The wave number of infrared spectra was ranging from (400 to 4000 cm-1). Thermogravimetric analysis (TGA) was conducted using a Shimadzu TGA- 50H instrument. The rate of heating was fixed at 10°C/min under a current of nitrogen flowing at a rate of 20 ml / min. The obtained (TGA) curves were recorded at temperature reaching to 800°C to measure the weight loss of the samples which exposed to elevated temperatures, at the Micro-Analytical Center, Cairo University, Giza, Egypt. The water of consistency and setting time of the geopolymer paste were carried out using standard Vicate Apparatus[26].

The compressive strength of all set specimens was measured by manually
compression testing machine (D550-control type, Milano-Italy) to determine the residual mechanical properties of the specimens after subjected to elevated temperatures and compared with those obtained from unheated samples at the age of 28 days.

## 3. Result and discussion

### *3.1. Water of consistency and setting time*

The standard water of consistency, initial and final setting times of geopolymer pastes are represented in Table 2. The results revealed that, the water of consistency increases with the addition of CKD as compared to the control mix ($M_0$). This is mainly due to the presence of alkalis and free lime as well as the high surface area of CKD leading to an increase in water demand [27]. It is noticed that both initial and final setting times are elongated in the sample $M_0$ which contain 100% MK. This in a good harmony with Mehena et al. [28], where they concluded that the higher levels of metakaolin can prolong the setting times. The addition of CKD leads to decrease the setting times of fresh geopolymer pastes. This may be attributed to the interaction of activated MK with free lime liberated from CKD which can accelerate the rate of hydration process. Consequently, the setting times become faster [14].

### *3.2. Characterization of metakaolin*

Fig. 1 displays the XRD diffractogram for the raw metakaolin. The XRD pattern shows a diffuse halo structure centered around 28.62º 2Θ, indicating the amorphous character of metakaolin and the

crystalline phase prevalent in the diffractogram is quartz ($SiO_2$) with basal reflections at (d=4.25 A$^o$ , d=3.34 A$^o$ close to 20.87$^o$ 2Θ and 26.64$^o$ 2Θ, respectively). Furthermore, some mineral phases such as illite ($KAl_2SiO_3AlO_{10}$ (OH) $_2$) at (d=9.33 A$^o$ near 10$^o$ 2Θ), microcline ($KAlSi_3O_8$) and traces of anatase ($TiO_2$) are exist as impurities in the X-ray patterns of metakaolin.

Fig. 2 shows the FTIR spectrum of the original metakaolin. The spectrum shows lowest absorption bands at 3433cm$^{-1}$ and 1620 cm$^{-1}$ which are ascribed to stretching and bending vibration modes of O-H and H-O-H, respectively. The main absorption band located at about 1087 cm$^{-1}$ correspond to the asymmetric stretching vibrations of Si-O and Al-O bonds, a shoulder band observed at 882 cm$^{-1}$ is assigned to out of-plane bending vibration of $CO_2$ which produced by atmospheric carbonation of clay particles, the symmetric stretching vibration of Si-O-Si was detected in the region 779-796 cm$^{-1}$. In the meantime, the band appears at approximately 693 cm$^{-1}$ is related to the symmetric stretching vibration of Si-O-Si and Si-O-Al(VI). Finally, the bending vibration mode of Si-O-Si and O-Si-O at approximately 463 cm$^{-1}$ represents quartz.

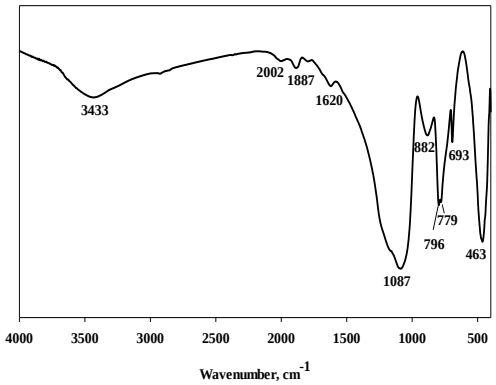


Fig. 2.IR spectrum of raw metakaolin

### *3.3. Fourier Transform infrared spectroscopy*

The FTIR spectra of geopolymer specimens ($M_0$, $MD_{20}$, $MD_{30}$ and $MD_{40}$) cured at ambient temperature for 28 days and after subjected to elevated temperatures 200, 400, 600 and 800°C are illustrated in Fig. 3(a-d). All spectra of geopolymer cements before heat treatment showed an increase in the intensity of absorption bands related to stretching vibration mode of O-H group at 3442-3460 cm$^{-1}$ and bending vibration mode of H-O-H at 1644-1649 cm$^{-1}$ when compared with the spectrum of initial metakaolin (Fig.2).

This indicates the dissolution and condensation of metakaolin species by using the alkalis present in CKD and the alkaline activator solution which leads to the formation of excessive amounts of hydration products within geopolymer matrix [29, 30]. Furthermore, the strong peak which attributed to asymmetric stretching vibration of Si-O-T where (T is Si or Al) that present in the IR spectrum of starting MK at 1087 cm$^{-1}$ (Fig. 2) shifted toward lower wave number around (~1000 cm$^{-1}$) for geopolymer mixes. This shift can be explained by the incorporation of Al ions in IV-fold coordination into Si-O-Si network leading to the formation of more Si-O-Al (IV) bridges [31, 32]. Also, the shift of the band can be interpreted as a result of the geopolymerization process and formation of amorphous aluminosilicate gels (C-S-H and N-(C)-A-S-H) in geopolymer binders. This is coherent with the intensity of bands at about 777 cm$^{-1}$ and 693 cm$^{-1}$ corresponding to symmetric stretching vibration of (Si-O-Si) and (Si-O-Si or Al-O-Si), respectively, which assert the completely dissolved of unreacted silica and the progress of the polymerization process [30].

Evidently, the intensity which is characteristic for anti-symmetric stretching vibration of Si-O-T band at 995-1040 cm$^{-1}$, in case of $MD_{20}$ mix is higher than those of other mixes as shown in Fig. 3b, suggesting that the addition of 20% CKD enhances the solubility of silica by the alkalis present in CKD and form highly crosslinked geopolymer gel. This is in a good agreement with Criado et al; Yang et al [33, 34] in which they stated that the stronger the intensity of the main asymmetric band, the higher the degree of polymerization.

While, further addition of CKD leads to increase the contribution of alkalis and chloride released from CKD resulting in the consumption of geopolymer surface and also increases in the crystallinity degree of hydration products. Increasing dust replacement leads to increase the intensity of carbonate peaks at 1430cm$^{-1}$, together with a distinct shoulder at 876 cm$^{-1}$. This is due to that the presence of significant amounts of alkalis, free lime and chloride in CKD caused a sort of crystalline products which in turn increases the open pores of the system and make the matrix more susceptible to carbonation [30].

Upon exposure to 200 and 400°C, all geopolymer samples show a sharp reduction in intensity of the T-O-T peak. This may be related to the decrease in the chain length of geopolymer [35, 36], which account for the regression of compressive strength between 200 and 400°C as mentioned in section 3.7. Also the intensity of bands attributed to water molecules at 3442-3460 $cm^{-1}$ and 1644- 1649 $cm^{-1}$ decreased after exposure to 200°C, indicating the evaporation of free and part of chemically bound water from the gepolymer matrix [37].This confirmed by the results observed in TGA analysis (Fig. 5). It is clear that, the bands at 1430 $cm^{-1}$ and 876 $cm^{-1}$, which are attributed to the carbonation of free alkalis started to diminish at 400°C and are completely vanished at 800°C [38]. There is a pronounced increase in the intensity of Si-O-T linkage for all geopolymer specimens at 600°C. This could be related to the further polymerization of unreacted metakaolin which promotes the densification of geopolymer [35, 36], which also is reflected in the residual strength values.

When raising the temperature to 800°C, the control mix $M_0$ shows a shoulder band at 1163 and 1079 $cm^{-1}$ are associated to asymmetric stretching mode of original metakaolin (Fig.2), as well as the wide band due to silicate phase splitting into three new absorption bands at 1078 $cm^{-1}$, 1013 $cm^{-1}$ and 928 $cm^{-1}$ for $MD_{40}$ geopolymer mix (Fig. 3d), implying the decomposition of (C-S-H and N-A-S-H) gel structure as a result of crystallization process [38, 39], and the formation of wollastonite phase which is emphasized by XRD patterns (Fig. 4d) and the peak observed at 780°C in TGA results (Fig. 5c). The most intensive band at 453 $cm^{-1}$ of bending vibration O-Si-O which is typical for geopolymer gel appeared as a series of peaks in IR spectra of $MD_{30}$ and $MD_{40}$ matrices. This is an evidence for disintegration of gel as well as the ordering of silicate network [40, 41].

On the contrary, there is no change observed in T-O-T bridge of $MD_{20}$ specimen after heating at 800°C, resulting from the viscous sintering which densified the matrix [42]. This coincides with the appearance of the small peak related to akermanite phase in XRD measurements (Fig. 4b), and also has been identified through TGA by observed peak between 700 -800°C, which it is typical for the collapse of zeolitic framework [43]. The represented data proved that the mix $MD_{20}$ containing 80% MK and 20% CKD possesses the high thermal stability of all geopolymer pastes.

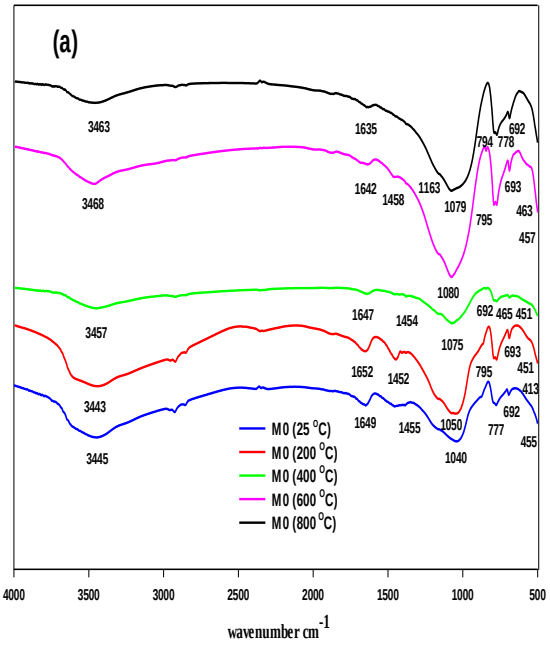


**Fig. 3a.**FTIR spectra of M0 geopolymer sample before and after exposure to different elevated temperatures

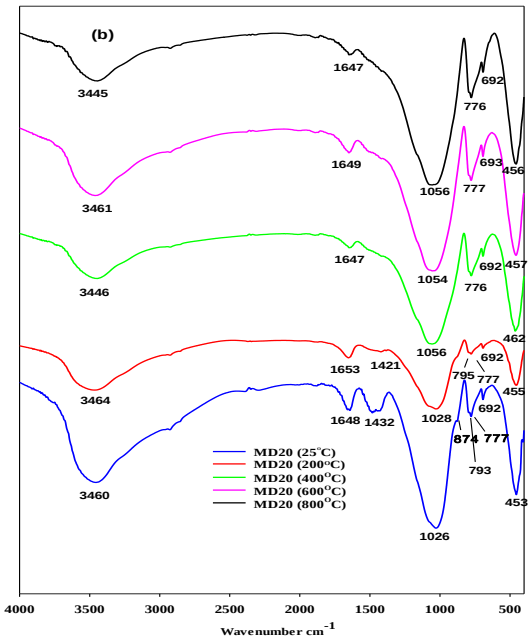


**Fig. 3b.**FTIR spectra of $MD_{20}$ geopolymer sample before and after exposure to different elevated temperatures

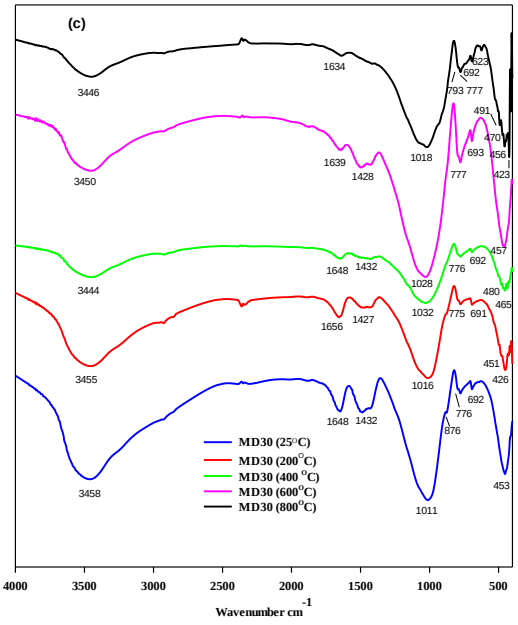


**Fig. 3c.**FTIR spectra of $MD_{30}$ geopolymer sample before and after exposure to different elevated

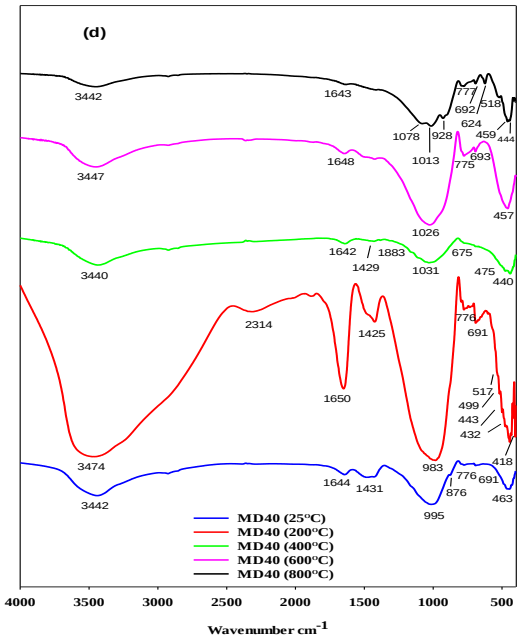


**Fig. 3d.**FTIR spectra of $MD_{40}$ geopolymer sample before and after exposure to different elevated

### *3.4. X-ray diffraction analysis (XRD)*

The XRD patterns for geopolymer specimens ($M_0$, $MD_{20}$, $MD_{30}$ and $MD_{40}$) at ambient temperature and after subjected to elevated temperatures 200, 400, 600 and 800°C are shown in Fig. 4(a-d), respectively. The XRD patterns of all activated samples before thermal treatment show huge and broad hump between (20-40º 2Ɵ), indicating the complete dissolution of metakaolin species as a result of alkaline activation and the formation of amorphous geopolymer matrix. It could be observed that the diffuse halo of the vitreous phase in the initial metakaolin (centered on 28.62º 2Ɵ) as shown in (Fig. 1) shifted slightly towards the higher degree (centered on 29.38º 2Ɵ) for all geoplymer samples. This shift has been described by Williams et al; Rickard et al, [44, 45] and implying the formation of amorphous aluminosilicate gel as a result of geopolymerization reaction.

The main crystalline phase has been identified as the primary product of geopolymerization process is (C-S-H) gel with the basal reflections at d=3.03 Aº , d=2.786 Aº close to 29.38º 2Ɵ, 32.09º 2Ɵ, respectively, where the dissolution of metakaolin leads to release free silica which is partially substituted with aluminium (Al) atoms or interacted with hydrated calcium oxide in CKD, suggesting the formation of new crystalline phase such as (C-(A)-S-H) type gel within the specimen. Indeed, quartz ($SiO_2$) is the dominant phase in all diffractograms of geopolymer pastes with the basal reflections (d=3.34, d=4.25 Aº). Moreover, other mineral phases which are present in the diffractogram of the original metakaolin such as anatase ($TiO_2$) at d=3.51Aº and the potassium feldspar microcline mineral ($KAlSi_3O_8$) at d=3.24Aº were observed in all geopolymer specimens after polymerization process. This implies that these minerals did not participate in the geopolymerization reaction. As can be seen in (Fig. 4b) of unheated $MD_{20}$ specimen with 20% addition of CKD, the stratlingite phase ($C_2ASH_8$) appeared at d=12.67Aº.

According to Silva et al. **[46]** the stratlingite phase is the main hydrated crystalline compound formed in paste with high MK content. Several authors **[47, 48]** reported that the presence of stratlingite confers a high mechanical strength to a lime-based material. The current study is agreement with these findings and manifested by the increase of the mechanical strength for $MD_{20}$ specimen as compared with the strength values of the other specimens.

The XRD patterns of all geopolymer cements after exposure to 200°C show a broad hump which is typical for N-(C)-A-S-H gel similar to that obtained from the unheated samples. This result is in a good harmony with the findings of Ruiz-Santaquiteria et al; Hussin et al **[49, 50]**. They concluded that the semi-crystalline (N-A-S-H) gel appeared in the geopolymer paste before and after thermal treatment at 200°C. However, the intensity of diffuse peak related to C-S-H around 2Ɵ =29.38º slightly decreased after exposure to 400°C; indicating the dehydration of gel **[51, 52]**. This confirms the reduction of compressive strength value between 200°C and 400°C. As the exposure temperature increased to 600°C, the diffuse peak at 2Ɵ =29.38º which starts to be reduced at 400°C almost completely disappeared. This is due to the destruction of C-S-H gel as a result of loss chemically bound water. However, the intensity of quartz peaks become progressively stronger for all geopolymer composites, implying the further polymerization of initially unreacted particles and reorganization of atoms resulting in an increase in the amorphous phase content and densification of the geopolymer matrix which promote a gradually strength gain after heating at 600°C.

Nevertheless, on further increase in elevated temperature to 800°C, more pronounced changes are observed in the diffraction patterns of all geopolymer samples. It was noticed that as the amorphous gel phase disappeared, new crystalline phases began to be generated. The diffractograms of both $MD_{30}$ and $MD_{40}$ geopolymer specimens after heating at 800°C (Fig. 4c and d) show the appearance of new diffraction peaks at d=2.97 Aº, d=2.63 Aº and d=1.86 Aº assigned to the formation of crystalline wollastonite phase ($CaSiO_3$). Also, the peak of kaolinite ($Al_2Si_2O_5(OH)_4$) was detected at d=7.47 Aº and d=4.01 Aº in control mix $M_0$ and also in mixes contain 30% and 40% CKD (Fig. 4a,c and d), respectively. This is more prominent with the appearance of a weak band at 518 $cm^{-1}$ only on the IR spectra of $MD_{40}$ (Fig. 3d) confirms the presence of kaolinite and the deconvolution of geopolymer gel, leading to the formation of more ordered structure. The expansion of crystalline phase is deemed to be the main reason for the presence of macro-cracks and damage of ($M_0$, $MD_{30}$ and $MD_{40}$) geopolymer specimens after heating to 800°C (Fig. 6) as well as the deterioration in strength. Meanwhile, the diffractogram of $MD_{20}$ specimen (Fig. 4b) exhibited the formation of akermanite phase ($Ca_2MgSi_2O_7$) at d=3.09Aº close to 28.86º 2Ɵ which was resulting from partial sintering of the remnant grains in the specimen. The viscous sintering acts as fillers and thus reinforces the structure. Rickard et al. **[21]** emphasize that the viscous sintering of the paste was the main factor that leads to increase the compressive strength in the geopolymers after firing as it released more of the aluminosilicate material from the unreacted particles into the binding phase and improved inter-particle connectivity. The XRD observations confirmed also the good thermal stability of geopolymer specimen with 20 wt% CKD.

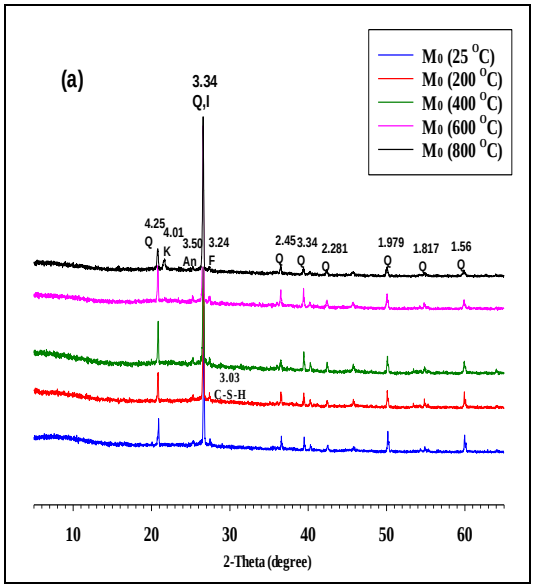


**Fig. 4a.** XRD pattern of $M_0$ geopolymer sample before and after heat exposure. An:anatase ($TiO_2$); F:feldspar ($KAlSi_3O_8$) ;Q:quartz ($SiO_2$); I:illite ($KAl_2SiO_3AlO_{10}(OH)_2$ ); K:kaolinite ($Al_2Si_2O_5(OH)_4$) ; calcium silicate hydrate: (C-S-H)

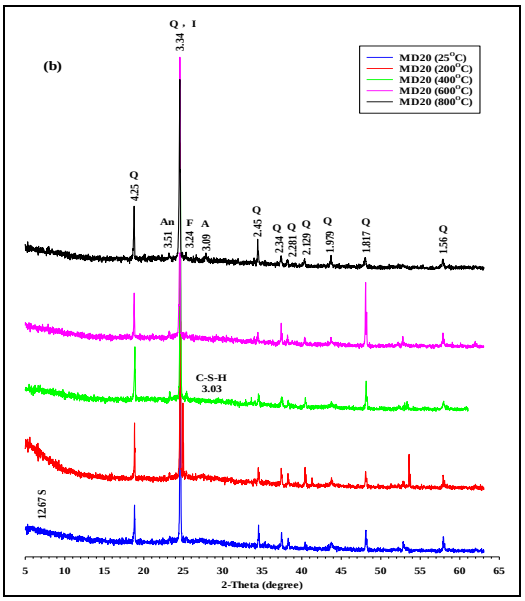


**Fig. 4b.**XRD pattern of $MD_{20}$ geopolymer sample before and after heat exposure. An:anatase ($TiO_2$); S: stratlingite ($C_2ASH_8$) ; F:feldspar ($KAlSi_3O_8$) ;Q:quartz ($SiO_2$); I:illite ($KAl_2SiO_3AlO_{10}$ $(OH)_2$ ); A:akermanite ($Ca_2MgSi_2O_7$);calcium silicate hydrate: (C-S-H)

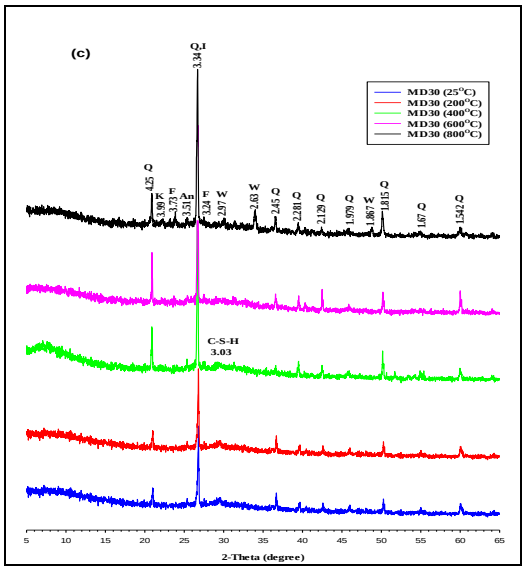


**Fig. 4c.** XRD pattern of $MD_{30}$ geopolymer sample before and after heat exposure. An:anatase ($TiO_2$); F:feldspar ($KAlSi_3O_8$) ;Q:quartz ($SiO_2$); I: illite ($KAl_2SiO_3AlO_{10}$ $(OH)_2$ ); K:kaolinite ($Al_2Si_2O_5(OH)_4$) ;w: wollastonite; ($CaSiO_3$) calcium silicate hydrate:(C-S-H)

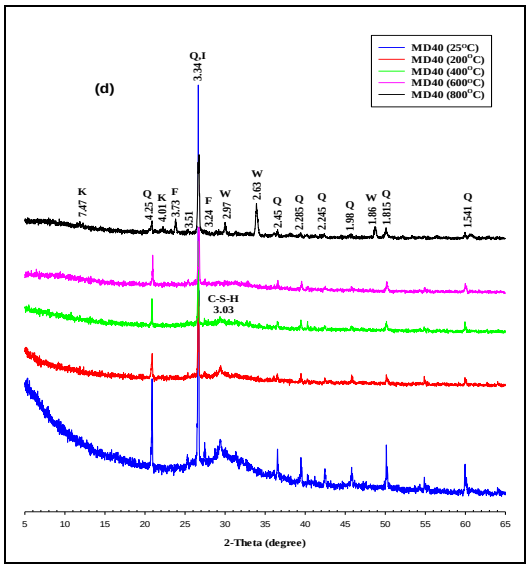


**Fig. 4d.** XRD pattern of $MD_{40}$ geopolymer sample before and after heat exposure. An:anatase ($TiO_2$); F:feldspar ($KAlSi_3O_8$) ;Q:quartz ($SiO_2$); I:illite ($KAl_2SiO_3AlO_{10}$ $(OH)_2$; K:kaolinite ($Al_2Si_2O_5(OH)_4$) ;W: wollastonite ($CaSiO_3$); calcium silicate hydrate: (C-S-H)

### *3.5. Thermogravimetric analysis (TGA/DTG)*

Fig. 5a-c represents the thermogravimetric analysis (TGA) and the derivative thermogravimetric analysis (DTG) for geopolymer samples ($MD_{20}$, $MD_{30}$ and $MD_{40}$) after 28 days of curing. The curves were used to determine the weight loss of geopolymers in the range of 30-800°C in order to study the thermal stability of the specimens before and after exposure to high temperatures.

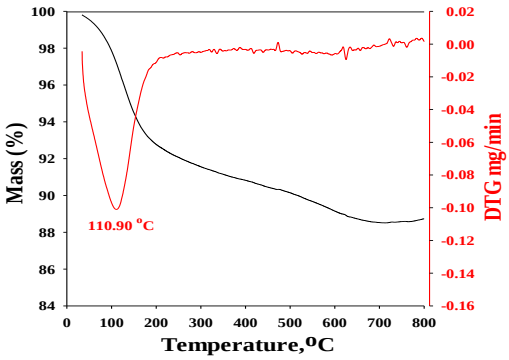


**Fig. 5a.**TGA and DTG curves of $MD_{20}$ geopolymer sample

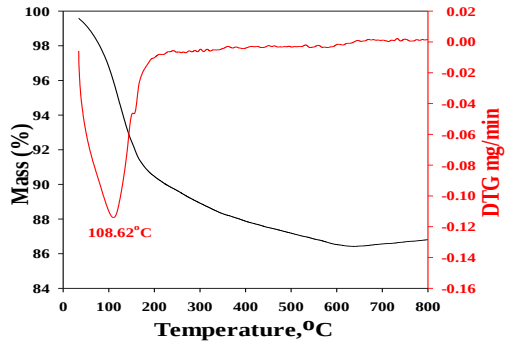


**Fig. 5b.**TGA and DTG curves of $MD_{30}$ geopolymer sample

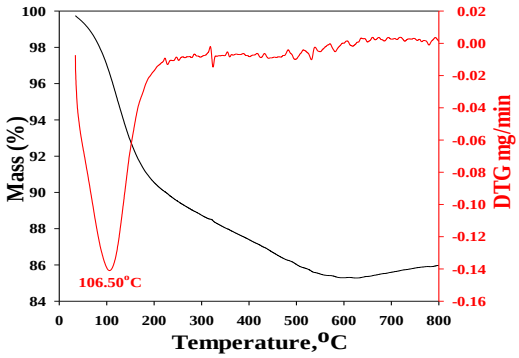


**Fig. 5c.**TGA and DTG curves of $MD_{40}$ geopolymer sample

The TGA/ DTG curves for all geopolymers show an endothermic peak span from an ambient temperature until 200°C, accompanied by a sharp reduction in mass. These are presumed to be due to the expelled of both free water and a part of tightly bounded water from the geopolymer structure **[18, 53]**. Furthermore, the most weight loss occurred below 200°C in all specimens and accounts for about 80% of the total mass loss **[54]**; this was mainly due to the rapid migration of the interstitial water towards the surface and then escape, which causes a damage to the internal microstructure of matrices and micro-cracks on the surface of geopolymer, and consequently a rapid degradation in the strength as discussed below (Fig. 7).

It is noteworthy that, the endothermic peak below 200°C for the composite containing 20wt% CKD (Fig. 5a) was shifted slightly to a higher temperature (110.90°C) than other samples. This proves that, the replacement of MK by 20 wt% CKD acts as a nucleating agent and filling the voids leading to form more tightly bound within the geopolymer gel. So, it results in producing a dense matrix **[55]**. While with a further increase in the CKD content up to 40 wt% (Fig. 5c), the endothermic peaks become steeper and shifted to lower temperature (106.50 °C). This is mainly due to that the excess amounts of CKD lead to increase the porosity in the matrix and reduce the ability of the sample to retain water **[56]**. The geopolymers continue to lose weight until 350°C with a total loss of about 8.85, 11.69 and 11.96% for $MD_{20}$, $MD_{30}$ and $MD_{40}$, respectively. This might be induced by dehydroxylation process of geopolymers.

There was a gradual mass loss (about 2%) under a slow rate between 350 and 650°C. This may be attributed to the dehydroxylation process and the formation of new T-O-T linkage that leads to densification of all matrices **[2]**. At this stage the small mass loss is probably due to the elimination of water which resulted from condensation of silanol or aluminol groups on the surface of geopolymer gel **[57]** as shown in equation (2) **[58].**

$$\equiv T\text{–}OH + OH\text{–}T \equiv \rightarrow \equiv T\text{–}O\text{–}T \equiv + H_2O \quad (2)$$

Where, T is (Al or Si) in tetrahedral sheets.

It can be seen from (Fig.5a) that the endothermic peak observed around 658°C in the mixture with 20 % CKD is more pronounced than that obtained from other geopolymer mixes ($MD_{30}$ and $MD_{40}$). This implies that the geopolymer composite containing MK in existence of 20% CKD have higher amounts of comprised gel and contain more tightly bound water within the matrix. Moreover, the DTG curve (Fig. 5c) for $MD_{40}$ mix shows a small exothermic peak at 780°C with a very little mass loss observed in the TG curve. The last exothermic peak may correspond to the destruction of amorphous C-S-H gel and the generation of the wollastonite crystalline phase as presented in the XRD analysis (Fig. 4d). On the other hand, the exothermic peak which detected only in the geopolymer specimen ($MD_{20}$) at the range of 700 - 800°C (Fig. 5a) with a minimal mass loss in the TGA data are characteristic for the collapse of zeolite structure **[43]**. The existing of this exothermic peak is related to the viscous sintering process as a result of the densification of geopolymer matrix **[21, 59]**, which can cause extreme strength when the

temperature exceeds 700°C. The masses remaining after heating all geopolymer samples to 800°C are 88.73, 87.24 and 86.26% for $MD_{20}$, $MD_{30}$ and $MD_{40}$, respectively. From this perspective, it is clear that the mixture containing 20wt% CKD have the highest thermal stability among all geopolymer samples.

### *3.6. Visual appearance*

Fig.6 (a-d) shows the physical observations with regard to the change of sample color and cracks development for unexposed and exposed geopolymer specimens to elevated temperatures of 200, 400, 600 and 800°C.


**Fig. 6a.**Physical observations of unexposed and exposed M0 geopolymer sample to elevated temperature


**Fig. 6b.**Physical observations of unexposed and exposed $MD_{20}$ geopolymer sample to elevated temperature

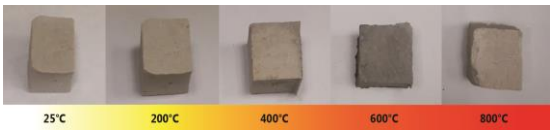


**Fig. 6c.**Physical observations of unexposed and exposed $MD_{30}$ geopolymer sample to elevated temperature

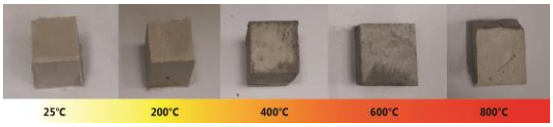


**Fig. 6d.**Physical observations of unexposed and exposed $MD_{40}$ geopolymer sample to elevated temperature

The visual inspection for all heated geopolymer cements indicated that the color of specimens unchanged from the original color (at 25°C) until 400°C. While after exposure to 600°C, the color of $M_0$, $MD_{30}$ and $MD_{40}$ samples (Fig. 6a, c and d) was impressively altered to dark grey. When the temperature increased to 800°C, the color of all samples becomes lighter. Moreover, hairline cracks were observed on the surface of all specimens accompanied by a strong linear shrinkage after heated to 200°C. This may be interpreted as, after exposure to 200°C the moisture loss become higher and the internal water try to escape out of the samples by forming pathways leave behind small pores distributed throughout the matrix **[60]**.

Meanwhile, the shrinkage which began to appear at 200°C become more intensive at 400°C due to the dehydroxylation process that can be taken place between 200 and 400°C, this consistent with the high volumetric contraction that can be observed in all samples after exposure to 400°C Fig. 6(a-d). The observation was supported by Zhang et al. **[61]**, where they studied the thermal behavior of geopolymer pastes after exposure to a high temperature and reported that the first maximum thermal shrinkage in geopolymer is due to the evaporation of free water occurred between 100-300°C at extremely higher rate, and beyond 300 °C the paste continues to shrink under a slow rate. It was found that, the higher shrinkage and the damage of geopolymer structure due to dehydroxylation was most probably responsible for the significant reduction of geopolymer strength in the temperature from 200°C to 400°C as previously reported by Tchakouté et al; Cheng-Yong et al **[18, 62].** Nevertheless, all samples heated at 600°C underwent structural changes due to the densification of unreacted silicate phase. This fact is in a good harmony with the gain of compressive strength at 600°C. Rahier et al. **[63]** reported that the temperature around 573°C and above is an indication of the glass transition temperature (Tg) and the densification of geopolymer paste.

On the other hand, after heating at 800°C, the samples of $M_0$, $MD_{30}$ and $MD_{40}$ were suffered from severe cracks and microstructural deterioration. This can be associated with the transformation of the amorphous gel into crystalline phase results in an unconstrained volume expansion which can cause wide cracks visually observed through the specimens as seen in (Fig. 6a, c and d). The existing of large cracks in geopolymer specimens leads to increase the likelihood of formation subverted and ruptured structure after thermal load, thus the strength loss was observed for these samples. Conversely, the $MD_{20}$ mix exhibited a much denser structure with fewer voids after exposure to 800°C (Fig. 6b). This suggested that the geoplymer gel sinters which allowed the viscous flow to fill voids present in the

structure **[54, 62, 64]**. The sintering and densification of geopolymer occur more significantly in 800°C than 600°C **[65]** and leads to a crack healing by intervening the geopolymer ingredients with each other and as such forming connected matrix **[54]**. It can be inferred that, the mix contain 80% MK and 20% CKD assisted in maintaining the dimensional stability, and hence improves the ability to resist the fire.

### *3.7. Compressive strength*

The compressive strength values of the geopolymer specimens cured at ambient temperature for 28 days and after heated at 200, 400, 600 and 800°C are shown in Fig. 7.

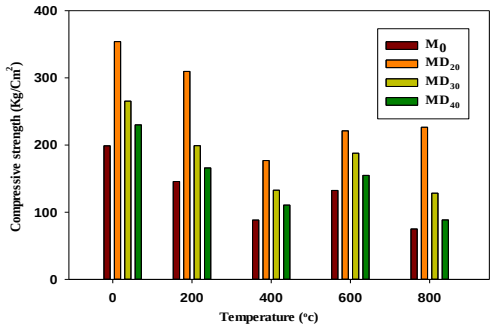


**Fig. 7.**Compressive strength of geopolymer samples before and after exposure to elevated temperatures.

The results indicated that, the mix $MD_{20}$ with 20% replacement of CKD achieved the maximum value of compressive strength as compared with the strength values of the other mixes at ambient temperature. This may be related to the interaction of MK with free lime (CH) liberated from CKD as well as the presence of alkalis within CKD leads to increase the dissolution rate of MK, providing the system with silicate and aluminate species, which complete the geopolymerization process as appeared from the higher intensity of geopolymer T-O-Si band (Fig. 3b). The increase of the reacted MK content is associated with the increase of the probability to form more hydration products such as C-S-H, C-A-H and N-(C)-A-S-H gel, which deposited in the open pores leading to increase the compressive strength. On the other hand, the replacement of CKD above 20% reduced the compressive strength of the mixes significantly. This is mainly attributed to the presence of large amounts of alkalis in the form of chloride and sulphate that causes a sort of crystalline hydrated products resulting in an opening of the pore system and so leads to lower the mechanical properties [29].

Generally, the increase of CKD content leads to transform the initially formed amorphous silicate gel into well crystalline phase (C-S-H) with a low mechanical strength [14].

As can be seen in Fig. 7, the residual compressive strength of all geopolymer matrices are decreased at 200°C as compared to the initial strength before heating. The reduction of strength from ambient temperature to 200°C was attributed to expel of the free water and a part of chemically bonded water from the geopolymer matrix, causing damage of Si-O-Si and Si-O-Al bonds and also decrease in the chain length of the geopolymer paste (as presented in section 3.3). The evaporation of water from the geopolymer structure could be responsible for the mass loss and the formation of micro cracks as a result of the thermal shrinkage during heating at 200°C (as discussed in the previous sections 3.5 and 3.6). Furthermore, after exposure to 400°C, the significant reduction in compressive strength values was observed when compared with non-exposed specimens of all geopolymer cements. This reduction of strength was related to the evaporation of chemically combined water from the structure in 100 -300°C range, followed by the dehydroxylation of the OH groups at a temperature above 300°C which induces the high shrinkage and accompanied by developing macro cracks in the geopolymer structure [43, 59].

Fig.7 indicates that all geopolymer samples show strength gained at 600°C. This can be mainly attributed to the polymerization of initially unreacted materials which leads to densify the matrix and increase T-O-Si band of all geopolymer at 600°C (as discussed in section 3.3 of FTIR analysis), resulting in an increase in the amorphous phase content (as seen clearly in section 3.4 of XRD analysis). However, after exposure to 800°C, a marked drop in strength was observed in $M_0$, $MD_{30}$ and $MD_{40}$ specimens. This could be related to the decomposition of aluminosilicate gel as a result of the loss of the total chemically bonded water. This causes a decrease in the residual strength of these samples, where the strength trend was well-agreed by

Tchakouté et al. [18].On the other hand, the strength increased slightly in $MD_{20}$ specimen after exposure to 800°C due to the viscous sintering process which occurred in the geopolymer mix at a temperature beyond 600°C which induced the healing of micro-cracks that led to a strength gain after exposure to 800°C [54] . According to the previous works [66, 67], the sintering effect leads to the formation of a very compact structure with a high mechanical strength by inducing crack healing and thus the specimens are well conserved from failure at elevated temperature. Therefore, the $MD_{20}$ specimen experienced the higher residual strength than control mix as well as other specimens containing CKD at 800°C.

## 4. Conclusions

The following conclusions can be drawn from the obtained results:

The addition of 20% CKD as a partial replacement of MK achieved the optimum compressive strength at ambient temperature compared with the control mix as well as other mixes containing CKD. This may be due to the formation of the additional (C-A-S-H) gel which fills the voids between grains leading to obtain a denser and stronger matrix.

All geopolymer pastes, the experienced loss in compressive strength from room temperature to 200°C is due to the dehydration of N-A-S-H gel, which in turn decreases the chain length of Si-O-Al and Si-O- Si bonds.

A sharp reduction in the compressive strength was observed in all geopolymer specimens after heating at 400°C followed by a rapid shrinkage and micro-cracks induced by dehydroxylation process.

All geopolymer pastes gained strength after thermal exposure to 600°C is due to the further polymerization of initially un-reacted materials leading to the formation of a dense matrix and improved the strength properties.

Geopolymer paste consisting of 80% metakaolin and 20% cement kiln dust enhanced the residual strength after exposure to 800°C due to the densification of matrix as a result of the viscous sintering process. This mix could have different applications at high temperatures.

## 5. Conflicts of interest

The authors declare that they have no known competing financial interests or personal relationships that could have appeared to influence the work reported in this paper “There are no conflicts to declare”.

## 6. Formatting of funding sources

This research did not receive any specific grant from funding agencies in the public, commercial, or not-for-profit sectors.

## 7. Acknowledgments

All facilities provided by Faculty of Women for Arts, Science and Education, Ain Shams University are greatly appreciated.

## 8. References

[1] H. Abdel-Gawwad, S. Abo-El-Enein, A novel method to produce dry geopolymer cement powder, HBRC journal 12(1) (2016) 13-24.
[2] L.R. Caballero, M.d.D.M. Paiva, E.d.M.R. Fairbairn, R.D. Toledo Filho, Thermal, Mechanical and Microstructural Analysis of Metakaolin Based Geopolymers, Materials Research 22(2) (2019).
[3] Y.J. Zhang, S. Li, Y.C. Wang, Microstructural and strength evolutions of geopolymer composite reinforced by resin exposed to elevated temperature, Journal of Non-Crystalline Solids 358(3) (2012) 620-624.
[4] O. Burciaga-Díaz, R. Magallanes-Rivera, J. Escalante-García, Alkali-activated slag-metakaolin pastes: strength, structural, and microstructural characterization, Journal of Sustainable Cement-Based Materials 2(2) (2013) 111-127.
[5] C. Nobouassia Bewa, H.K. Tchakouté, D. Fotio, C.H. Rüscher, E. Kamseu, C. Leonelli, Water resistance and thermal behavior of metakaolin-phosphate-based geopolymer cements, Journal of Asian Ceramic Societies 6(3) (2018) 271-283.
[6] M. Salimi, A. Ghorbani, Mechanical and compressibility characteristics of a soft clay stabilized by slag-based mixtures and geopolymers, Applied Clay Science 184 (2020) 105390.
[7] X. Yao, Z. Zhang, H. Zhu, Y. Chen, Geopolymerization process of alkali–metakaolinite characterized by isothermal calorimetry, Thermochimica Acta 493(1-2) (2009) 49-54.

[8] A. Nmiri, N. Hamdi, M. Duc, E. Srasra, Synthesis and characterization of kaolinite-based geopolymer: alkaline activation effect on calcined kaolinitic clay at different temperatures, Journal of Materials and Environmental Sciences 8(2) (2017) 276-290.
[9] Z. Zhang, H. Wang, Y. Zhu, A. Reid, J.L. Provis, F. Bullen, Using fly ash to partially substitute metakaolin in geopolymer synthesis, Applied Clay Science 88 (2014) 194-201.
[10] P. Rovnaník, K. Šafránková, Thermal behaviour of metakaolin/fly ash geopolymers with chamotte aggregate, Materials 9(7) (2016) 535.
[11] M.A. Villaquirán-Caicedo, R.M. de Gutiérrez, S. Sulekar, C. Davis, J.C. Nino, Thermal properties of novel binary geopolymers based on metakaolin and alternative silica sources, Applied Clay Science 118 (2015) 276-282.
[12] K.V. Teja, T. Meena, A.N. Reddy, Investigation on Metakaolin and Silicafume Incorporated Concrete under Elevated Temperature, IJCMS 7 (2018).
[13] S. Abo-El-Enein, M. Heikal, M. Amin, H. Negm, Reactivity of dealuminated kaolin and burnt kaolin using cement kiln dust or hydrated lime as activators, Construction and Building Materials 47 (2013) 1451-1460.
[14] M.R. Shatat, G.A. Ali, G.A. Gouda, Effect of hydrothermal curing on hydration characteristics of metakaolin–CKD pastes at different temperatures in a closed system, Beni-Suef University journal of basic and applied sciences 5(4) (2016) 299-305.
[15] M. Frías, J. Cabrera, Pore size distribution and degree of hydration of metakaolin–cement pastes, Cement and Concrete Research 30(4) (2000) 561-569.
[16] P. De Silva, F.P. Glasser, Phase relations in the system CaO□ Al2O3□ SiO2□ H2O relevant to metakaolin-calcium hydroxide hydration, Cement and concrete research 23(3) (1993) 627-639.
[17] A.M. Rashad, A.A. Hassan, S.R. Zeedan, An investigation on alkali-activated Egyptian metakaolin pastes blended with quartz powder subjected to elevated temperatures, Applied Clay Science 132 (2016) 366-376.
[18] H.K. Tchakouté, C.H. Rüscher, S. Kong, E. Kamseu, C. Leonelli, Thermal behavior of metakaolin-based geopolymer cements using sodium waterglass from rice husk ash and waste glass as alternative activators, Waste and biomass valorization 8(3) (2017) 573-584.
[19] A. Elimbi, H. Tchakoute, M. Kondoh, J.D. Manga, Thermal behavior and characteristics of fired geopolymers produced from local Cameroonian metakaolin, Ceramics International 40(3) (2014) 4515-4520.
[20] V.F. Barbosa, K.J. MacKenzie, Thermal behaviour of inorganic geopolymers and composites derived from sodium polysialate, Materials research bulletin 38(2) (2003) 319-331.
[21] W.D. Rickard, J. Temuujin, A. van Riessen, Thermal analysis of geopolymer pastes synthesised from five fly ashes of variable composition, Journal of non-crystalline solids 358(15) (2012) 1830-1839.
[22] A. Elimbi, H. Tchakoute, D. Njopwouo, Effects of calcination temperature of kaolinite clays on the properties of geopolymer cements, Construction and Building Materials 25(6) (2011) 2805-2812.
[23] A. ASTM, Standard test method for compressive strength of hydraulic cement mortars (using 2-in. or [50-mm] cube specimens), Annual Book of ASTM StandardsAnnual Book of ASTM Standards 4(1) (2013) 1-9.
[24] N. Saikia, A. Usami, S. Kato, T. Kojima, Hydration behaviour of ecocement in presence of metakaolin, Resources Processing 51(1) (2004) 35-41.
[25] H. Khater, S.R. Zedane, Geopolymerization of industrial by-products and study of their stability upon firing treatment, International Journal of Engineering and Technology 2(2) (2012) 308-316.
[26] A. Designation, C191: Standard test method for normal consistency and setting time of Hydraulic Cement ", Annual Book of ASTM Standards (2008) 172-174.
[27] S.A. El-Aleem, M. Abd-El-Aziz, M. Heikal, H. El Didamony, Effect of cement kiln dust substitution on chemical and physical properties and compressive strength of Portland and slag cements, The Arabian Journal for Science and Engineering 30(2 B) (2005).
[28] O. Mehena, I. Amar, J. Raoul, Strength and setting times of metakaolincement-based geopolymer pastes, American Journal of Civil and Environmental Engineering 2(4) (2017) 30-36.
[29] H. Khater, Effect of cement kiln dust on geopolymer composition and its resistance to sulfate attack, Green Materials 1(1) (2013) 36-46.
[30] H. Khater, M. Ezzat, A. El Nagar, Engineeri ng of Low Cost Geopolymer Building Bricks Applied For Various Construction Purposes, International Journal of Civil Engineering and Technology 7(4) (2016).
[31] S.J. Melele, H.K. Tchakouté, C. Banenzoué, E. Kamseu, C.H. Rüscher, F. Andreola, C. Leonelli, Investigation of the relationship between the condensed structure and the chemically bonded water content in the poly (sialate-siloxo) network, Applied Clay Science 156 (2018) 77-86.
[32] H.I. Riyap, C.N. Bewa, C. Banenzoué, H.K. Tchakouté, C.H. Rüscher, E. Kamseu, M.C. Bignozzi, C. Leonelli, Microstructure and mechanical, physical and structural properties of sustainable lightweight metakaolin-based geopolymer cements and mortars employing rice husk, Journal of Asian Ceramic Societies 7(2) (2019) 199-212.

[33] M. Criado, A. Fernández-Jiménez, A. Palomo, Alkali activation of fly ash: Effect of the SiO2/Na2O ratio: Part I: FTIR study, Microporous and mesoporous materials 106(1-3) (2007) 180-191.
[34] Z. Yang, R. Mocadlo, M. Zhao, R.D. Sisson Jr, M. Tao, J. Liang, Preparation of a geopolymer from red mud slurry and class F fly ash and its behavior at elevated temperatures, Construction and Building Materials 221 (2019) 308-317.
[35] G. Mathew, B. Joseph, MICROSTRUCTURAL ANALYSIS OF FLY ASH BASED GEOPOLYMER EXPOSED TO ELEVATED TEMPERATURES, Acta Technica Corvininesis-Bulletin of Engineering 10(2) (2017).
[36] S. Luhar, S. Chaudhary, I. Luhar, Thermal resistance of fly ash based rubberized geopolymer concrete, Journal of Building Engineering 19 (2018) 420-428.
[37] O. Burciaga-Díaz, J. Escalante-García, R. Magallanes-Rivera, Compressive strength and microstructural evolution of metakaolin geopolymers exposed at high temperature, Revista ALCONPAT 5(1) (2015) 58-72.
[38] P. Rovnaník, P. Bayer, P. Rovnaníková, Characterization of alkali activated slag paste after exposure to high temperatures, Construction and Building Materials 47 (2013) 1479-1487.
[39] S. Bernal, E. Rodríguez, R. Mejía de Gutiérrez, J.L. Provis, Performance at high temperature of alkali-activated slag pastes produced with silica fume and rice husk ash based activators, Materiales de construcción 65(318) (2015).
[40] W. Mozgawa, J. Deja, Spectroscopic studies of alkaline activated slag geopolymers, Journal of Molecular Structure 924 (2009) 434-441.
[41] I. Lancellotti, M. Catauro, C. Ponzoni, F. Bollino, C. Leonelli, Inorganic polymers from alkali activation of metakaolin: Effect of setting and curing on structure, Journal of Solid State Chemistry 200 (2013) 341-348.
[42] M. Lahoti, K.K. Wong, E.-H. Yang, K.H. Tan, Effects of Si/Al molar ratio on strength endurance and volume stability of metakaolin geopolymers subject to elevated temperature, Ceramics International 44(5) (2018) 5726-5734.
[43] P. Duxson, G.C. Lukey, J.S. van Deventer, Physical evolution of Na-geopolymer derived from metakaolin up to 1000 C, Journal of Materials Science 42(9) (2007) 3044-3054.
[44] R.P. Williams, R.D. Hart, A. Van Riessen, Quantification of the Extent of Reaction of Metakaolin- Based Geopolymers Using X- Ray Diffraction, Scanning Electron Microscopy, and Energy- Dispersive Spectroscopy, Journal of the American Ceramic Society 94(8) (2011) 2663-2670.
[45] W.D. Rickard, L. Vickers, A. Van Riessen, Performance of fibre reinforced, low density metakaolin geopolymers under simulated fire conditions, Applied Clay Science 73 (2013) 71-77.
[46] A.S. Silva, A. Gameiro, J. Grilo, R. Veiga, A. Velosa, Long-term behavior of lime–metakaolin pastes at ambient temperature and humid curing condition, Applied Clay Science 88 (2014) 49-55.
[47] J. Ding, Y. Fu, J. Beaudoin, Strätlingite formation in high alumina cement-silica fume systems: significance of sodium ions, Cement and Concrete Research 25(6) (1995) 1311-1319.
[48] M. Heikal, M.M. Radwan, M.S. Morsy, Influence of curing temperature on the Physico-mechanical, Characteristics of Calcium Aluminate Cement with air cooled Slag or water cooled Slag, Ceramics-Silikáty 48(4) (2004) 185-196.
[49] C. Ruiz-Santaquiteria, J. Skibsted, A. Fernández-Jiménez, A. Palomo, Alkaline solution/binder ratio as a determining factor in the alkaline activation of aluminosilicates, Cement and Concrete Research 42(9) (2012) 1242-1251.
[50] M. Hussin, M. Bhutta, M. Azreen, P. Ramadhansyah, J. Mirza, Performance of blended ash geopolymer concrete at elevated temperatures, Materials and Structures 48(3) (2015) 709-720.
[51] C. Alonso, L. Fernandez, Dehydration and rehydration processes of cement paste exposed to high temperature environments, Journal of materials science 39(9) (2004) 3015-3024.
[52] S.M. Park, J.G. Jang, N. Lee, H.-K. Lee, Physicochemical properties of binder gel in alkali-activated fly ash/slag exposed to high temperatures, Cement and Concrete Research 89 (2016) 72-79.
[53] D.L. Kong, J.G. Sanjayan, Effect of elevated temperatures on geopolymer paste, mortar and concrete, Cement and concrete research 40(2) (2010) 334-339.
[54] W.D. Rickard, Assessing the suitability of fly ash geopolymers for high temperature applications, Curtin University, 2012.
[55] A. Nikolov, I. Rostovsky, H. Nugteren, Geopolymer materials based on natural zeolite, Case Studies in Construction Materials 6 (2017) 198-205.
[56] H. Assaedi, F. Shaikh, I.M. Low, Effect of nano-clay on mechanical and thermal properties of geopolymer, Journal of Asian Ceramic Societies 4(1) (2016) 19-28.
[57] H. Hao, K.-L. Lin, D. Wang, S.-J. Chao, H.-S. Shiu, T.-W. Cheng, C.-L. Hwang, ELUCIDATING CHARACTERISTICS OF GEOPOLYMER WITH SOLAR PANEL WASTE GLASS, Environmental Engineering & Management Journal (EEMJ) 14(1) (2015).
[58] P. Duxson, A. Fernández-Jiménez, J.L. Provis, G.C. Lukey, A. Palomo, J.S. van Deventer, Geopolymer technology: the current state of the art, Journal of materials science 42(9) (2007) 2917-2933.

[59] O.A. Abdulkareem, A.M. Al Bakri, H. Kamarudin, I.K. Nizar, A.S. Ala'eddin, Effects of elevated temperatures on the thermal behavior and mechanical performance of fly ash geopolymer paste, mortar and lightweight concrete, Construction and building materials 50 (2014) 377-387.
[60] M. Lahoti, K.H. Tan, E.-H. Yang, A critical review of geopolymer properties for structural fire-resistance applications, Construction and Building Materials 221 (2019) 514-526.
[61] H.Y. Zhang, V. Kodur, B. Wu, L. Cao, F. Wang, Thermal behavior and mechanical properties of geopolymer mortar after exposure to elevated temperatures, Construction and Building Materials 109 (2016) 17-24.
[62] H. Cheng-Yong, L. Yun-Ming, M.M.A.B. Abdullah, K. Hussin, Thermal resistance variations of fly ash geopolymers: foaming responses, Scientific reports 7(1) (2017) 1-11.
[63] H. Rahier, J. Wastiels, M. Biesemans, R. Willlem, G. Van Assche, B. Van Mele, Reaction mechanism, kinetics and high temperature transformations of geopolymers, Journal of materials science 42(9) (2007) 2982-2996.
[64] S. Alehyen, M. Zerzouri, M. ELalouani, M. Achouri, M. Taibi, Porosity and fire resistance of fly ash based geopolymer, Journal of Materials and Environmental Sciences 9 (2017) 3676-3689.
[65] A. Mustafa Al Bakri, O.A. Abdulkareem, H. Kamarudin, I. Khairul Nizar, A. Rafiza, Y. Zarina, A. Alida, Microstructure Studies on the Effect of the Alkaline Activators of Fly Ash-Based Geopolymer at Elevated Heat Treatment Temperature, Applied Mechanics and Materials, Trans Tech Publ, 2013, pp. 342-348.
[66] W.D. Rickard, A. Van Riessen, Performance of solid and cellular structured fly ash geopolymers exposed to a simulated fire, Cement and Concrete Composites 48 (2014) 75-82.
[67] K. Zulkifly, H. Yong, M. Abdullah, L. Ming, D. Panias, K. Sakkas, Review of geopolymer behaviour in thermal environment, Iop Conference Series: Materials Science and Engineering, IOP Publishing, 2017, p. 012085.